A&A, 685, A151 (2024)
https://doi.org/10.1051/0004-6361/202348918

Astronomy & Astrophysics

The metal-poor edge of the Milky Way's "thin disc"

Emma Fernández-Alvar[1,2,3], Georges Kordopatis[3], Vanessa Hill[3], Giuseppina Battaglia[1,2], Carme Gallart[1,2], Isaure González Rivera de la Vernhe[3], Guillaume Thomas[1,2], Federico Sestito[4], Anke Ardern-Arentsen[5], Nicolas Martin[6,7], Akshara Viswanathan[8], and Else Starkenburg[8]

[1] Departamento de Astrofísica, Universidad de La Laguna, 38206 La Laguna, Tenerife, Spain
e-mail: emmafalvar@gmail.com
[2] Instituto de Astrofísica de Canarias, 38200 La Laguna, Tenerife, Spain
[3] Université Côte d'Azur, Observatoire de la Côte d'Azur, CNRS, 06300 Laboratoire Lagrange, France
[4] Department of Physics & Astronomy, University of Victoria, Victoria, BC V8P 1A1, Canada
[5] Institute of Astronomy, University of Cambridge, Madingley Road, Cambridge CB3 0HA, UK
[6] Université de Strasbourg, CNRS, Observatoire astronomique de Strasbourg, UMR 7550, 67000 Strasbourg, France
[7] Max-Planck-Institut für Astronomie, Königstuhl 17, 69117 Heidelberg, Germany
[8] Kapteyn Astronomical Institute, University of Groningen, Landleven 12, 9747 AD Groningen, The Netherlands

Received 12 December 2023 / Accepted 16 February 2024

ABSTRACT

Context. The emergence of the disc in our Galaxy and the relation between thick and thin disc formation and evolution is still a matter of debate. The chemo-dynamical characterization of disc stars is key to resolving this question, particularly at parameter regimes, where both disc components overlap, such as the region around [Fe/H] ~ −0.7 corresponding to the thin disc's metal-poor end.

Aims. In this paper, we re-assess the recent detection of a metal-poor extension of stars moving with thin-disc-like rotational velocities between −2 < [Fe/H] < −0.7, carried out on the basis of metallicity estimates obtained from photometric data and their rotational velocity distributions.

Methods. We explored the chemo-dynamical properties of metal-poor stars from the recent *Gaia* third data release (DR3), which includes the first catalog of metallicity estimates from the Radial Velocity Spectrometer (RVS) experiment. We complemented them with the two largest high-resolution ($\lambda/d\lambda > 20\,000$) spectroscopic surveys available: the GALAH DR3 and the APOGEE DR17.

Results. We confirm that there are high-angular-momentum stars moving in thin-disc-like orbits, that is, with a high angular momentum of $L_z/J_{\rm tot} > 0.95$, and close to the Galactic plane, $|Z_{\rm max}| < 750$ pc, reaching metallicity values down to [Fe/H] ~ −1.5. We also find tentative evidence for stars moving on such orbits at lower metallicities, down to [Fe/H] ~ −2.5, albeit in smaller numbers. Based on their chemical trends, thin-disc-like stars with [Fe/H] < −1 would have formed in a medium that is less chemically evolved than the bulk of the thick disc. Stars with chemical abundances typical of the thin disc appear at metallicities between −1 < [Fe/H] < −0.7.

Key words. Galaxy: abundances – Galaxy: disk – Galaxy: formation – Galaxy: kinematics and dynamics – Galaxy: stellar content

1. Introduction

Analyses of the Milky Way (MW) have clearly established that most stars in our Galaxy move in a disc configuration following a double density law, leading to a separation into distinct thin and thick disc components (Gilmore & Reid 1983). Over recent decades, further chemo-dynamical analysis have revealed that both components are also differentiated both chemically (e.g., in the [α/Fe] vs. [Fe/H] abundance space; see Fuhrmann 1998; Bensby et al. 2003; Reddy et al. 2003) and dynamically, ending up distributed in different proportions over the Galactic plane and from the Galactic center (Jurić et al. 2008; Kordopatis et al. 2015; Hayden et al. 2015; Queiroz et al. 2020).

Thin-disc stars, that is, those moving closer to the plane with low eccentricities, display an overall low [α/Fe] enhancement and a metallicity distribution centered around the solar value (Recio-Blanco et al. 2014; Hayden et al. 2014), which ranges from supersolar values down to [Fe/H] ~ −0.7 on its metal-poor end (Bensby et al. 2014; Fuhrmann et al. 2017). On the contrary, the thick disc reaches larger distances from the plane, rotating with a lower angular momentum. Its stars show a higher [α/Fe] enhancement and a poorer metallicity content than the thin disc, with a broader metallicity distribution centered around [Fe/H] ~ −0.55 (Gilmore et al. 1989; Katz et al. 2011; Kordopatis et al. 2011b) extending towards much lower values – several works have even reported the identification of a very metal-poor population moving in orbits compatible with the thick disc, the so-called metal-weak thick disc, down to metallicities [Fe/H] ~ −2.5 (Norris et al. 1985; Beers et al. 2002; Ruchti et al. 2011; Kordopatis et al. 2013; Carollo et al. 2019), although its link with the more metal-rich thick disc is still a matter of debate (Mardini et al. 2022). Even if the chemo-dynamical properties of the thin and the thick discs are generally different, there is a large overlap between them and the thin and thick disc classification based on their chemistry does not correspond precisely to the classification based on their dynamics (e.g., Bensby et al. 2014). This fact makes it difficult to understand the disc components origin.

Cosmological simulations of Milky-Way-like galaxies point to several formation scenarios that could explain the double disc characteristics: the formation of a dynamically hot disc after an early stage of turbulent accretion of stellar substructures into the Milky Way halo (e.g., Jones & Wyse 1983; Brook et al. 2004; Bird et al. 2013) or the formation of the thick disc from

dynamical heating of a thinner component caused by mergers of satellite galaxies into the Galaxy (Quinn et al. 1993; Font et al. 2001; Villalobos & Helmi 2008, among others) or by depositing stars (Abadi et al. 2003). To this day, it is not clear when the thin disc started forming. In any case, the first stages of Galaxy formation seem to have been dominated by a high merger activity (El-Badry et al. 2018), which would have prevented the formation of a disc that would be stable over time. Thus, finding old stars (and, consequently, those with a very low metallicity content) moving in cold disky orbits is unexpected and puzzling.

Recent studies have found more and more evidence of very ([Fe/H] < −2), extremely ([Fe/H] < −3), and even ultra-metal-poor stars ([Fe/H] < −4), with a large angular momentum and a location that is confined relatively close to the Galactic plane (Sestito et al. 2019, 2020, 2021; Di Matteo et al. 2020; Venn et al. 2020; Cordoni et al. 2021; Dovgal et al. 2024), most of them moving in thick-disc-like orbits. Sestito et al. (2021) and Santistevan et al. (2021) investigated their possible origin with cosmological simulations, concluding that some of the stars from accreted structures that merged early (and became the building blocks of the Milky Way) and/or later mergers heading in specific directions would end up on relatively planar orbits. Another kind of explanation was recently proposed by Dillamore et al. (2024). By exploring particle simulations these authors showed that a rotating bar can give the stellar halo a net spin, leading to an asymmetric prograde angular momentum distribution with some stars moving close to the plane on disc-like orbits. Yuan et al. (2023) and Li et al. (2023) also presented how due to a rapidly decelerating bar, some bulge stars gain rotation because they are trapped in co-rotating regions and move outwards on prograde planar orbits. However, they concluded that the fraction of stars affected by this mechanism is too small to account for all the metal-poor rotators detected. Thus, their origin is still unclear.

A recent analysis by Fernández-Alvar et al. (2021; hereafter FA21) of stars observed as part of the Pristine survey (Starkenburg et al. 2017; Martin et al. 2023) towards the Galactic anticenter revealed a stellar population moving with rotational velocities that are not just disc-like, but typical of the thin disc at metallicities down to [Fe/H] ∼ −2. The metallicities used in the FA21 analysis were derived photometrically with the Pristine filter centered on the CaHK doublet at ∼3900 Å, which is very sensitive to a variation of the global metallicity of the star. The aim of the present work is to verify, with more accurate spectroscopic metallicities and a more complete dynamical characterization, the existence of high angular-momentum stars at very low metallicities (−2 < [Fe/H] < −0.7) and investigate their possible linked origin with the chemically defined thin disc (i.e., the low-[α/Fe] population).

The *Gaia* third data release (DR3; Gaia Collaboration 2016, 2023) provides the first determinations of stellar parameters and chemical abundances obtained from the Radial Velocity Spectrometer (RVS; Cropper et al. 2018; Recio-Blanco et al. 2023). This is the largest existing sample of stellar parameters and individual abundances homogeneously derived for Milky Way stars from medium-resolution spectra ($\lambda/\mathrm{d}\lambda \sim 11\,500$). It comprises a database of 5.6 million stars, including several 10^4 stars with [Fe/H] < −1. Combined with the highly accurate astrometric measurements, this constitutes a extremely valuable sample to explore the metal-poor tail of the thin disc. In addition, we also investigated the two largest high-resolution spectroscopic surveys available, the GALAH DR3 ($\lambda/\mathrm{d}\lambda \sim 28\,000$; Buder et al. 2021) and APOGEE DR17 ($\lambda/\mathrm{d}\lambda \sim 22\,500$; Abdurro'uf et al. 2022).

This paper is structured as follows. We present the data and the quality selection criteria applied in Sect. 2. We explore the metallicity distribution function (MDF), chemical abundance trends and orbital parameters of dynamically selected thin-disc-like stars in Sect. 3. Finally, we summarize and discuss our results in Sect. 4.

2. Data selection

We selected stars within the *Gaia* DR3 RVS, GALAH DR3 and APOGEE DR17 spectroscopic databases with estimated metallicities lower than [Fe/H][1] < −0.55, where the probability of finding stars in thin disc orbits is very low based on the standard thin disc MDF (e.g., Bensby et al. 2014), even considering the disc metallicity gradients with both radial and vertical distance (∼−0.06 ± 0.00 dex kpc^{-1} and ∼−0.26 ± 0.01 dex kpc^{-1}, respectively – e.g. Kordopatis et al. 2020; Imig et al. 2023).

We searched for the best-quality data among the *Gaia* DR3 RVS database by following the selection suggested by Recio-Blanco et al. (2023) for metal-poor stars (see their Sect. 10.5). Their criteria, which include flags and parameter constraints, are meant to avoid possible incorrect metallicity estimates due to the T_{eff}-[M/H] degeneracy induced by the upper limit on T_{eff} in the training grid in their analysis. Apart from the criteria they provided, we conservatively included additional constraints to reject hot and cool stars for which the metallicity determination could be less reliable also because of their proximity with the limits of the *GSP-Spec* model grid. Thus, we removed stars reported in the "Astrophysical parameters" table as *spectraltype_esphs* types O, B, and A. We restricted our stars to stellar parameters between $4250 < T_{\mathrm{eff}}$ [K] < 6000 and $0 < \log g < 4.75$; and we considered only stars with the *flag_extrapol* < 2. We provide a table of all the flags and conditions we applied in Appendix A. We calibrated the RVS metallicities with the $\log g$ dependent third-order polynomial suggested by Recio-Blanco et al. (2023) and keep stars with calibrated metallicities lower than [Fe/H] < −0.55.

Because of the small wavelength range covered by the RVS spectra and the fact that it is dominated by the Ca II triplet (at 8498 Å, 8542 Å and 8662 Å), some degeneracies between the [Fe/H] and [α/Fe] determinations could lead to systematic errors when deriving these chemical abundances (e.g. Kordopatis et al. 2011a; Matsuno et al. 2022). For instance, an overestimation of [α/Fe] would translate in underestimating [Fe/H]. In that case, some metal-rich thin-disc stars could contaminate our sample of interest, below [Fe/H] < −1. These would show large [α/Fe] enhancements. We evaluated this issue by comparing the *Gaia* RVS [Fe/H] of our selected sample with the [Fe/H] of stars in common within GALAH and APOGEE databases. The comparison showed that we avoid underestimated [Fe/H] by removing stars at [Fe/H] > −2, with *flags_gspspec* chain character number 7 equal to 2. The details of this comparison are shown in Appendix B.

For the GALAH data, we filtered out those with unreliable stellar parameters (*flag_sp* = 0) and with unreliable metallicities (*flag_fe_h* = 0), as suggested by Buder et al. (2021). During our analysis, we detected a decreasing trend of the metallicity

[1] Both *Gaia* RVS and APOGEE provide two sets of iron abundances: [M/H], calculated using all the spectral range available, and [Fe/H], estimated by taking into account only individual iron lines. In this work we consider the [M/H] parameter. In the case of GALAH they only provide a unique set of [Fe/H] values. For convenience, we will refer to them all as [Fe/H] from now on.

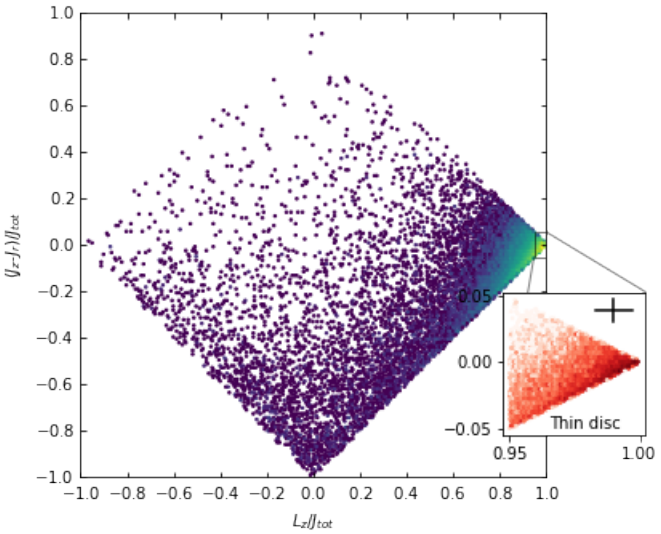

Fig. 1. Action space (normalized to the sum of the three actions of motion, J_{tot}) of *Gaia* RVS stars with calibrated [Fe/H] < −0.55, along with a zoom-in of the area that we use to select our thin disc sample. The x axis displays the normalized angular momentum, which is equivalent to the azimuthal action of motion and the y axis the normalized difference of vertical action and radial action. Their mean uncertainties are displayed in black on the top right corner.

with $T_{\rm eff}$ in stars with $T_{\rm eff} > 6500$ K. Overestimating $T_{\rm eff}$, for example because of a sub-optimal broadening model, would lead to a substantial underestimation of [Fe/H]. To avoid this problem, we focused on cooler stars only and rejected those with $T_{\rm eff}$ differences between photometric and spectroscopic determinations (both provided by the GALAH Collaboration – Buder et al. 2021) larger than 300 K. We added an additional cut removing stars with a large velocity broadening, $v_{\rm broad} > 15\,{\rm km\,s^{-1}}$, which could be related to unresolved binaries or fast spinning stars, and would also lead to inaccurate [Fe/H] measurements[2].

In the case of APOGEE data, we selected only stars with ASPCAPFLAG bits 14–42 equal to 0, STARFLAG bits 1–26 equal to 0, and EXTRATARG bits 2 and 4 equal to 0. We also excluded those objects with the *apogee*1*_target*1, *apogee*1*_target*2, *apogee*2*_target*1, and *apogee*2*_target*2 classifying them as clusters[3], streams, dwarf galaxies, sky, telluric, binaries, radial velocity variables, the bar, extended objects, and the TriAnd, GASS, and A13 disc structures. In addition, we select only stars with $3500 < T_{\rm eff}\,[{\rm K}] < 6500$ and $1 < \log g\,[{\rm dex}] < 3.5$, where the determination of stellar parameters, including metallicity, are more reliable (Jönsson et al. 2020). For consistency with the *Gaia* RVS final metallicity upper limit, we restricted our GALAH and APOGEE samples to stars with [Fe/H] < −0.55.

To select stars in thin-disc-like orbits (see Sect. 3) we consider the actions of motion of the stars, J_r, J_ϕ, and J_z[4], which are invariants with time (for a static potential in a galaxy in equilibrium) and can offer a better classification of the stellar motion than present day velocities. We also evaluate their rotational velocity, V_ϕ, maximum distance from the plane reached in their orbits, $|Z_{\rm max}|$, and guiding radius, $R_{\rm guide}$[5]. We derived the velocities and actions of motion as in Kordopatis et al. (2023; see their Sect. 3.1) considering the spectroscopic *Gaia* RVS/GALAH/APOGEE radial velocities, *Gaia* DR3 proper motions and distances calculated by Bailer-Jones et al. (2021).

We imposed some additional quality data cuts to minimize parameter uncertainties that may result in non-physical properties for some disc stars. To remove possible binaries, we discarded the stars for which the measured GALAH/APOGEE radial velocity is not in agreement with the *Gaia* measurement, within the uncertainties. We also excluded likely binaries based on the *Gaia* ruwe parameter (ruwe > 1.4, as suggested by Lindegren et al. 2021). We restrict ourselves to precise distances by removing stars with parallax relative uncertainties greater than 20%. Finally, we did not take into account those for which our final total velocity exceeds the escape velocity of the Galaxy, $600\,{\rm km\,s^{-1}}$, calculated using the McMillan (2017) potential as in Kordopatis et al. (2023). These selection criteria resulted in samples of 41682 *Gaia* DR3 RVS stars, 21544 GALAH DR3 stars, and 16404 APOGEE DR17 stars.

3. Metal-poor stars on thin-disc orbits

Figure 1 represents the combined vertical and radial actions $(J_z - J_r)$ as a function of the azimuthal action L_z, normalized to the sum of the three, $J_{\rm tot} = J_z + |L_z| + J_r$. The stars of interest, that is, moving on circular orbits on the Galactic plane, would be those with $L_z/J_{\rm tot} \sim 1$ and $(J_z - J_r)/J_{\rm tot} \sim 0$. We select stars on thin-disc-like orbits by choosing those with $L_z/J_{\rm tot} > 0.95$, which have a $|(J_z - J_r)/J_{\rm tot}| < 0.05$. This selection still includes some stars reaching large distances from the plane (up to $|Z_{\rm max}| \sim 3$ kpc; see left panel of Fig. 2). To restrict our sample to be consistent with the location where most of the Pristine stars in FA21 were observed, we only keep stars with $|Z_{\rm max}| < 1.5$ kpc. While this threshold might appear as too generous, we recall that the relative proportion of thin-disc stars at $|Z_{\rm max}| \sim 1.5$ kpc at the solar radius is still of the order of 50 percent (e.g., Jurić et al. 2008, however, see also Vieira et al. 2023). We note however, that depending on the radial dependence of the scale-height of each of the discs, this ratio may be different at different radii (see Bland-Hawthorn & Gerhard 2016 for a discussion). That said, based on Fig. 2, we can see that most of our targets are confined within $|Z_{\rm max}| < 750$ pc, which is consistent with the limits of the geometrical thin disc (with a scale height of 300 pc measured in the solar neighborhood; Bland-Hawthorn & Gerhard 2016). The analysis below confirms that the bulk of these stars indeed display $|Z_{\rm max}|$ values that are significantly lower than this 1.5kpc limit, irrespective of their metallicity.

We obtained 12889 *Gaia* DR3 RVS stars, 4097 GALAH DR3 stars, and 1840 APOGEE DR17 stars that fulfill our orbital and chemical criteria: $L_z/J_{\rm tot} > 0.95$, $|Z_{\rm max}| < 1.5$ kpc and [Fe/H] < −0.55, including the specific quality selection applied to each survey explained in Sect. 2. Among those, there are 211 stars in common between *Gaia* RVS and APOGEE, 211 between *Gaia* RVS and GALAH, and only 9 in common between the three surveys. As expected based on the selection criteria, the eccentricities, *ecc*, of the resulting samples are very low,

[2] For *Gaia* RVS metallicities, this issue was taken care of via the $v_{\rm broad}$ flags as shown in Appendix A.

[3] We also verified the presence of cluster members considering the candidates published in Hunt & Reffert (2023). We found only 18 in *Gaia* RVS, 9 in GALAH, and 8 in APOGEE, all of them with [Fe/H] > −1, except for 1 APOGEE star with [Fe/H] = −1.38. Thus, the presence of these objects is extremely low and do not have an impact on the action space distribution of our thin-disc-like sample.

[4] J_ϕ is identical to the angular momentum, L_z. We will refer to it as L_z from now on.

[5] $R_{\rm guide} = (R_{\rm apo} + R_{\rm peri})/2$, being $R_{\rm apo}$ and $R_{\rm peri}$ the apocenter and pericenter of a stellar orbit, respectively.

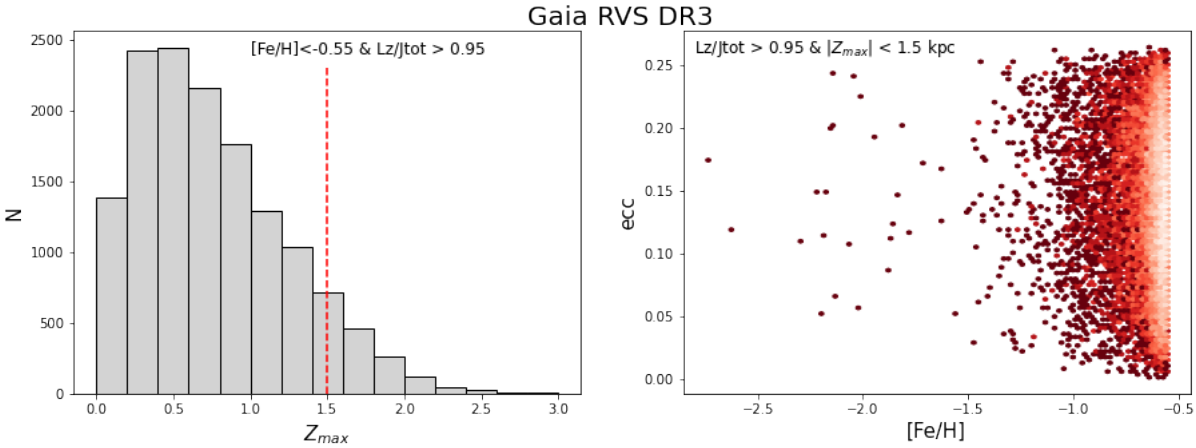

Fig. 2. $|Z_{\rm max}|$ distribution of the *Gaia* RVS DR3 stars with [Fe/H] < -0.55 and $L_z/J_{\rm tot} > 0.95$ (left). The red dashed line at $|Z_{\rm max}| = 1.5$ kpc correspond to the upper limit that we impose to avoid stars that reach very large distances from the Galactic plane. Eccentricities distribution of the our final thin disc selection: stars with $L_z/J_{\rm tot} > 0.95$ and $|Z_{\rm max}| < 1.5$ kpc (right).

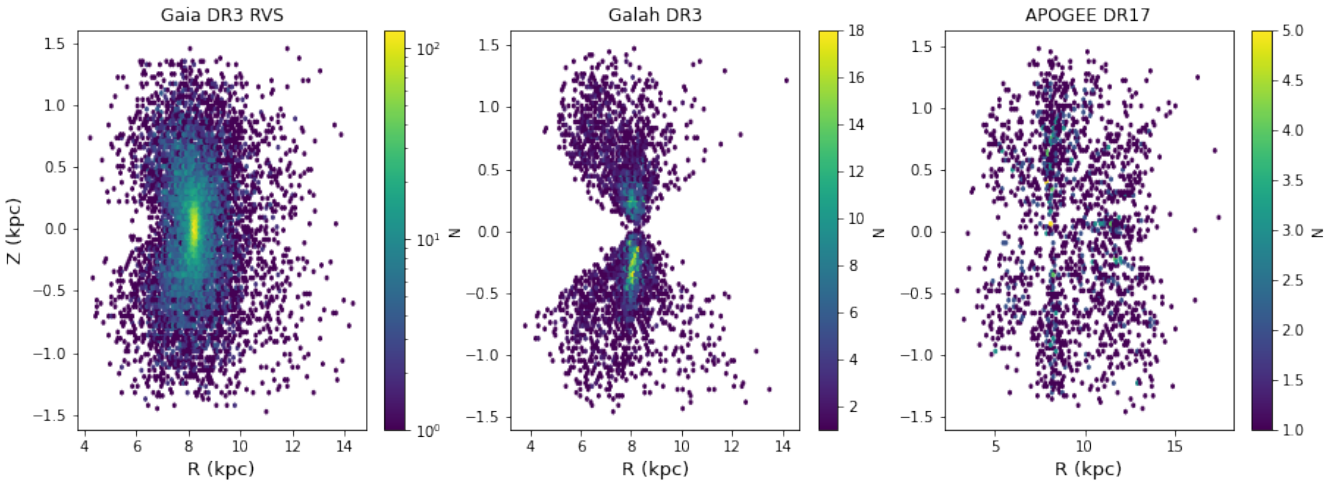

Fig. 3. Spatial distribution in cylindrical galactocentric coordinates of our thin disc samples selected in *Gaia* RVS (left), GALAH (middle), and APOGEE (right).

distributing uniformingly between $0 < ecc < 0.3$ and showing no trends with metallicity (see right panel of Fig. 2).

Figure 3 displays the spatial distribution of our thin-disc selected stars with [Fe/H] < -0.55 gathered within *Gaia* DR3 RVS, GALAH DR3, and APOGEE DR17. The location of the selected thin-disc stars is different depending on the survey, with *Gaia* DR3 RVS covering more evenly the Galactocentric radii between 6 and 10 kpc and distance from the plane between -1.5 and 1.5 kpc, thus including the anticenter explored by FA21. APOGEE stars cover a similar area, but GALAH stars clearly avoid the anticenter.

3.1. Metallicity distribution and orbital characterization.

We derived the metallicity distribution function (MDF) of our selected thin-disc-like stars, which are displayed in the left panels of Fig. 4 on a logarithmic scale[6]. The top panel corresponds to the MDF for our final selection with $|Z_{\rm max}| < 1.5$ kpc and the bottom panel shows the MDF of those stars that reach only up to $|Z_{\rm max}| < 750$ pc, which resembles the previous one, although the lack of stars below [Fe/H] < -1.5 dex is more evident for the latter. We assess the impact of the orbital parameters uncertainties on the selection. Right panels of Fig. 4 show the MDFs after excluding all the stars for which the orbital parameters uncertainties leave them out of the dynamical selection described above (considering their higher limit uncertainty). This excludes 296, 423, and 212 from the *Gaia* RVS, GALAH, and APOGEE thin-disc-like samples, respectively. The resulting MDFs show a similar shape as the left panels of Fig. 4, albeit the stricter selection.

The three surveys show similar MDFs: a continuous decrease down to [Fe/H] ~ -1.5 and, albeit in much lower numbers, the existence of high-angular-momentum stars down to [Fe/H] ~ -2.5. To make a quantitative comparison of the MDFs of the three surveys, the percentage of stars below -1, -1.5, and -2, with respect to those below -0.55 (and $|Z_{\rm max}| < 1.5$ kpc), are shown in Table 1. The coherence in the MDFs derived from surveys that used different methodologies to determine stellar metallicities confirms the existence of this fast rotating metal-poor tail. In addition, the detection of this population does not depend on the specific selection functions of these three surveys nor on a particular location in the Galaxy, as it is shown

[6] The MDF derived with APOGEE data is already cleaned from stars with a likely accreted origin, as suggested by their chemical trends (see Sect. 3.2).

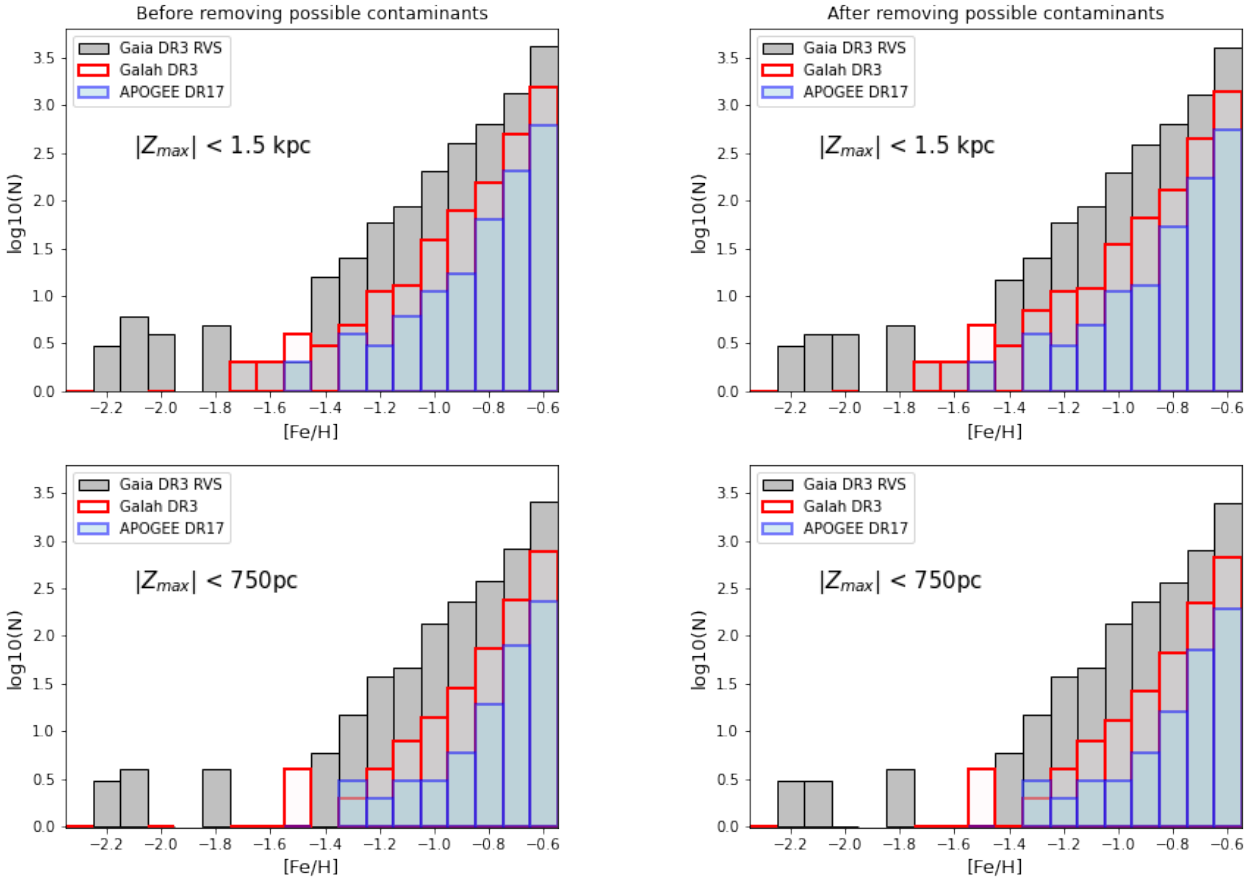

Fig. 4. Metallicity distribution functions, in logarithmic scale, derived from our thin disc samples of *Gaia* DR3 RVS, GALAH, and APOGEE stars (left). Right panels are the same as the left, but excluding stars for which the uncertainties on their orbital parameters leave them out of the selection criteria.

Table 1. Number of stars below [Fe/H] < −0.55, −1, −1.5, and −2 and the corresponding percentage (in brackets) with respect to the number of stars with [Fe/H] < −0.55.

Survey	<−0.55	<−1	<−1.5	<−2
Gaia RVS	12889	415 (3.22)	27 (0.21)	15 (0.12)
GALAH	4097	80 (1.95)	10 (0.24)	2 (0.05)
APOGEE	1788	26 (1.45)	2 (0.11)	0 (0)

in Fig. 3. In particular, they are not restricted to the anticenter region, where FA21 had detected them initially.

Top panels in Fig. 5 show the stellar orbital rotational velocity as a function of metallicity. This is the parameter space in which FA21 identified the potential metal-poor thin-disc tail. The three top panels show (from left to right) all stars with [Fe/H] < −0.55 in *Gaia* DR3 RVS, GALAH DR3, and APOGEE DR17 (after the quality selection). The metal-poor thin-disc-like stars are overplotted in a red density scale, on top of the gray density scale that shows the complete metal-poor sample. Contour plots of the 50%, 75%, 90%, 99%, and 99.9% (the latter only for our thin-disc-like sample) are overplotted following the same color code.

The distributions of our three selected samples resemble qualitatively the one displayed in FA21: a large fraction between −0.55 and −1.5, and a significant drop at lower metallicities. However, contrary to what was observed in FA21, the number of stars below −1.5 is much lower. This fact could be due to a large fraction of underestimated [Fe/H] within the Pristine photometric metallicity catalog that would be artificially increasing the number of stars down to [Fe/H] ∼ −2 (see González-Rivera et al., in prep.). Another explanation could be that the stars with high V_ϕ in Pristine do not enter the strict thin disc selection based on actions applied in the present work. Either way, the number of stars detected in these surveys that move in thin-disc-like orbits at metallicities below [Fe/H] < −1.5 is very low, compared with the rest of the stellar sample at the same metallicity.

The following rows in Fig. 5 show the distributions of V_ϕ, $|Z_{\rm max}|$, and $R_{\rm guide}$ (from top to bottom, respectively) in four different metallicity ranges (−1 < [Fe/H] < −0.5, −1.5 < [Fe/H] < −1, −2 < [Fe/H] < −1.5 and [Fe/H] < −2). We see that the V_ϕ distributions do not strongly depend on the metallicity range considered and they are compatible with a thin-disc velocity distribution ($\langle V_\phi \rangle \sim 240\,{\rm km\,s^{-1}}$ – GRAVITY Collaboration 2019), although the stellar velocity distribution at −1 < [Fe/H] < −0.55 peaks at slightly higher velocities than stars at lower metallicities.

There is a large fraction of stars with −1 < [Fe/H] < −0.55 confined closer than 500 pc from the plane and at lower metallicities the peak of the distribution moves slightly towards larger $|Z_{\rm max}|$, around 500–750 pc, although some stars are also very close to the plane, with $|Z_{\rm max}| \sim 100$ pc. Even if the $|Z_{\rm max}|$ upper limit of 1.5 kpc imposed in our selection criteria is a bit large to be considered a geometric thin disc, looking at the resulting $|Z_{\rm max}|$ distributions we confirm that most of our stars are confined in thin-disc-like orbits, very close to the plane.

Because of our criteria selecting stars in almost circular orbits, the $R_{\rm guide}$ must be similar to their current galactocentric radius and, thus, their distributions depend on the selection

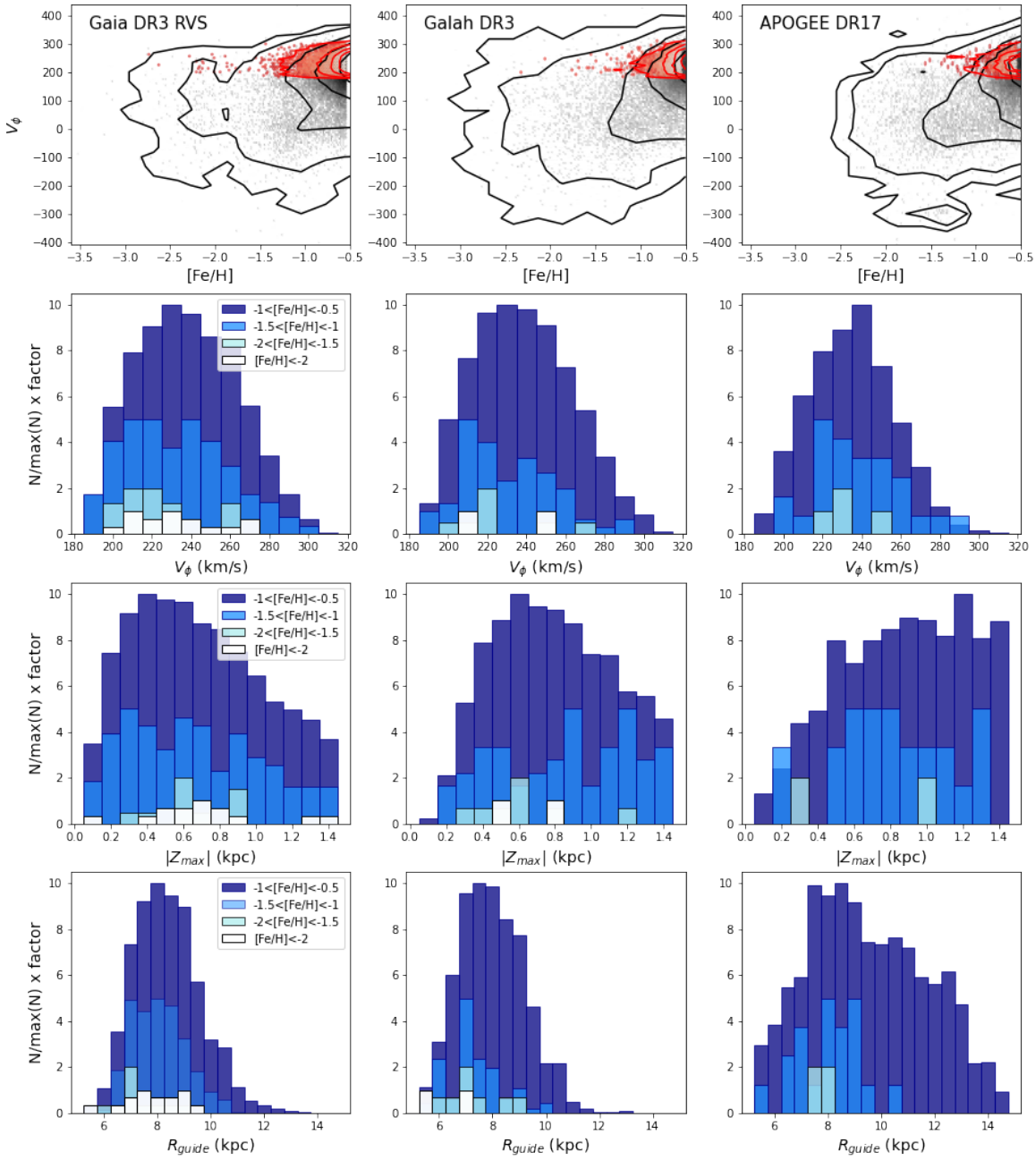

Fig. 5. Rotational velocity, V_ϕ, as a function of the metallicity, [Fe/H], color coded by density scale, for the thin disc selections (top row). Thin-disc stars are shown in red scale overplotted over the rest of the sample in grey scale. Contour plots of the 50%, 75%, 90%, 99%, and 99.9% (the latter only for the metal-poor thin disc) are overplotted following the same color code. Second row: V_ϕ distributions of thin-disc stars at four different ranges of metallicity (from dark blue to white, [Fe/H] < -0.5, [Fe/H] < -1, [Fe/H] < -1.5, [Fe/H] < -2), normalized to the maximum number of stars and multiplied by a factor to help the visualization (from dark blue to white, ×10, ×5, ×2 and ×1). Third and fourth rows: same as middle panels but for $|Z_{\rm max}|$ and $R_{\rm guide}$ distributions, respectively. From left to right we display the *Gaia* DR3 RVS, GALAH and APOGEE stellar samples.

function of each survey. APOGEE covers larger distances than the other surveys towards the outer disc. Interestingly, it shows that metal-rich stars $R_{\rm guide}$ reach up to 14 kpc but stars at [Fe/H] < -1 are confined within radius below ~10 kpc, as if they did not actually belong to the outer disc.

3.2. Chemical trends to shed light on their origin

As mentioned before, previous studies have shown that at metallicities [Fe/H] > -0.7, Milky Way stars moving in thick-disc-like orbits tend to have high-[α/Fe] ratios (chemical thick disc), and stars moving in thin-disc-like orbits show low-[α/Fe] ratios (chemical thin disc). Figure 6 displays the [α/Fe] vs. [Fe/H] space for stars in the three surveys following our thin disc selection criteria, at all [Fe/H]. APOGEE abundances clearly show that our high angular-momentum selection is not only comprised by the low-α population, but there is also a fraction of high-α stars; there are also some stars with a very low [α/Fe] content, [α/Fe] ~ -0.2, which may point to an accreted origin (Tolstoy et al. 2009; Das et al. 2020). Both GALAH and *Gaia*

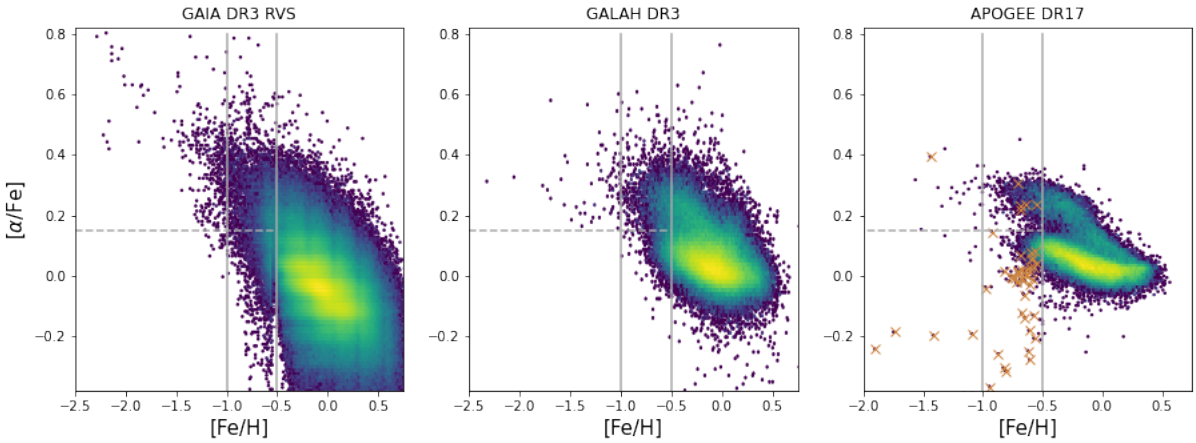

Fig. 6. [α/Fe] ratios as a function of [Fe/H] estimates derived from *Gaia* RVS (left panel), GALAH (middle panel), and APOGEE (right panel) for stars at all metallicities moving in thin-disc-like orbits based on our selection criteria. Two grey lines at [Fe/H] = −0.5 and [Fe/H] = −1 help to visualize the location of our metal-poor thin-disc stars in this chemical space. The grey dashed line at 0.15 indicates the separation in high- and low-α. Golden yellow crosses in the APOGEE panel correspond to stars with a likely accreted origin (see Sect. 3.2) that we exclude in our chemo-dynamical analysis of thin-disc-like stars (Figs. 4 and 5).

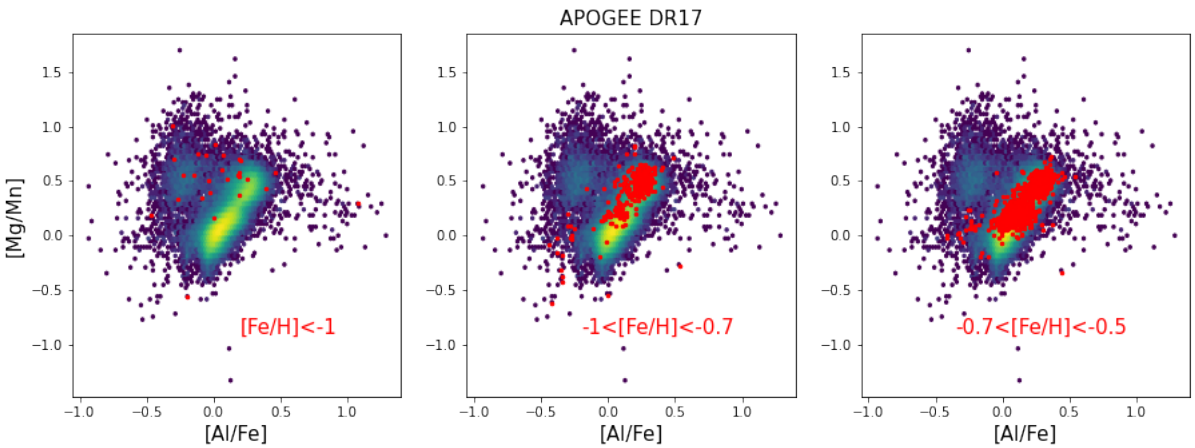

Fig. 7. [Mg/Mn] vs. [Al/Fe] chemical ratios of APOGEE stars verifying our selection criteria, color coded based on the stellar density. Overplotted in red are our selected thin-disc-like sample with metallicities below [Fe/H] < −1 (left panel), −1 < [Fe/H] < −0.7 (middle panel), and −0.7 < [Fe/H] < −0.55 (right panel).

RVS show consistent trends with APOGEE, although more scattered and not split into two sequences[7]. for the latter.

We roughly separated the stars into high-α and low-α, following the observed split in the APOGEE abundances at [α/Fe] ~ 0.15. The three catalogs show that among stars with −1 < [Fe/H] < −0.55, around 50% are high- and low-α, but below [Fe/H] < −1, most of our stars tend to be high-α.

We also explore the [Mg/Mn] versus [Al/Fe] which is another chemical space where the Galactic components also differentiate chemically (Hawkins et al. 2015; Horta et al. 2021). In their Fig. 2, Horta et al. (2021) illustrated the chemical evolution followed by a Milky-Way-like system and a GES-like galaxy on this space. The upper left region is populated by the first stars formed in both systems, when the chemical enrichment is still early and unevolved. Later, due to a fast but intense star formation rate, the Milky Way follows an increase of [Al/Fe] due to the contribution of AGBs while the [Mg/Mn] remains high (thick disc) and then, once the SNIa explode, both the [Mg/Mn] and [Al/Fe] decrease (thin disc). On the other hand, a system such GES, which had a slower SFH (Fernández-Alvar et al. 2018), starts the chemical evolution in the upper left region and as the metallicity increases, the [Al/Fe] increases slowly and remains subsolar, while the [Mg/Mn] decreases (Andrews et al. 2017).

We focus on the APOGEE abundances, for which the differences between the components are more clearly visible. Figure 7 shows the whole sample of thin-disc-like stars at all metallicities as in Fig. 6, color-coded in density scale, overplotted with those in our sample with metallicities below [Fe/H] < −1 (left panel), between −1 < [Fe/H] < −0.7 (middle panel), and −0.7 < [Fe/H] < −0.55 (right panel) in red. We see that stars with [Fe/H] < −1 clearly populate the upper left region associated to the early star formation when the stellar populations were chemically unevolved. As the metallicity increases the number of stars populating the thick disc region dominates; however, there are stars populating the thin disc region, even at metallicities below −0.7. At higher metallicities, both locations are well populated. Interestingly, at metallicities [Fe/H] > −1, there is a group of stars that follows the expected chemical evolution path of a dwarf satellite (lower-left region). These stars

[7] This is likely due to the fact that GSPspec's alpha is mostly a [Ca/Fe] measurement, which does not separate high-alpha and low-alpha populations clearly (see Prantzos et al. 2023; Mikolaitis et al. 2014.

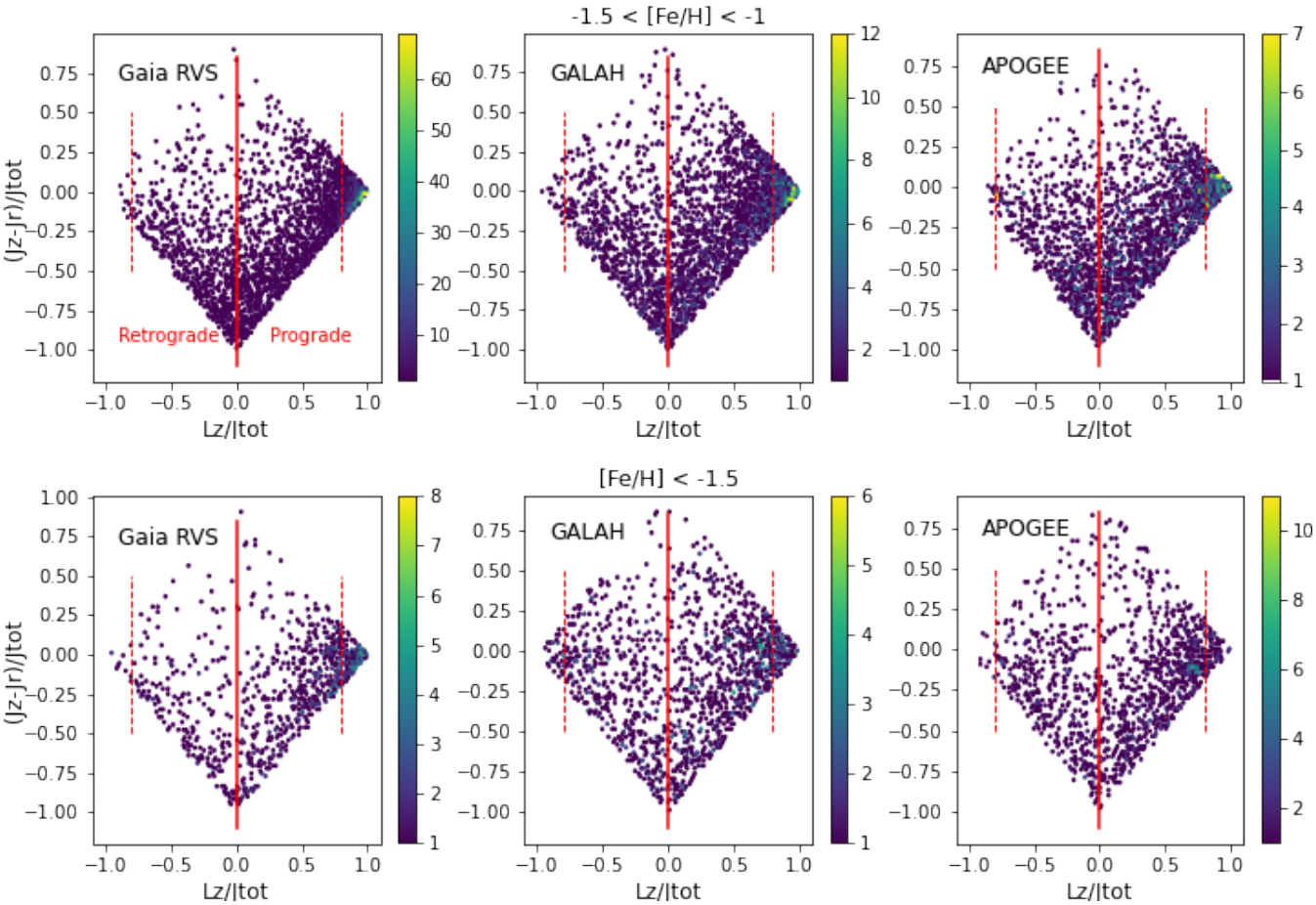

Fig. 8. Action space as in Fig. 1 of stars with metallicities between $-1.5 < [\mathrm{Fe/H}] < -1$ (top panels) and below $[\mathrm{Fe/H}] < -1.5$ (bottom panels), within the *Gaia* RVS DR3 (left), GALAH DR3 (middle), and APOGEE DR17 (right) databases. A continuous red line separate stars moving on prograde (L_z/J_{tot}) and retrograde (L_z/J_{tot}) orbits. Red dashed lines mark at $L_z/J_{\mathrm{tot}} = 0.8$ and -0.8 mark the most prograde and most retrograde ends of the distributions.

have also low [α/Fe] content. Thus, they are likely candidates of being accreted stars and we excluded them to derive the MDF in Fig. 4.

Chemical abundances derived with automatic pipelines that run on hundreds of thousands of stars should be taken with a grain of salt, since they are not thoroughly tested on peculiar cases as the one investigated in this paper. For this reason we checked the APOGEE spectra of our selected thin-disc-like stars with $[\mathrm{Fe/H}] < -1$ to verify that the spectral fit with models from which the chemical abundances were derived are reliable. We only detected one star, with APOGEE_ID "2M08401826+5145470", $S/N = 52$, $[\mathrm{Fe/H}] = -1.317$ and $[\alpha/\mathrm{Fe}] = 0.419585$, with extreme flux values in some of the pixels and whose Fe lines are deeper than the solution fit, pointing to an underestimated [Fe/H]. However, the spectra of the vast majority have a signal-to-noise ratio (S/N) that is higher than 100 and show a good fit between each observation and its best model solution, giving us confidence in our results.

In summary, based on these chemical abundance distributions of the stars we observed at $[\mathrm{Fe/H}] < -0.55$ moving in thin-disc-like orbits, we conclude that the chemo-dynamically defined thin disc begins to appear at metallicities between -1 and -0.7. At lower metallicities, the thin-disc-like stars exhibit chemical abundances that point to a star formation in a system that is chemically unevolved and less enriched than the bulk of the thick disc.

3.3. Investigating a thin disc, thick disc, or a prograde halo origin

The present analysis confirms the existence of stars moving in thin-disc-like orbits below $[\mathrm{Fe/H}] < -0.55$ down to $[\mathrm{Fe/H}] < -1.5$ and even lower metallicities, although in fewer numbers. However, their chemical trends show that not all of them are part of the chemical thin disc. In particular, at metallicities $[\mathrm{Fe/H}] < -1$ they present the chemical signature characteristic of an early chemical enrichment, distinct from the thick disc. In addition, given their paucity, we were not able to rule out that these stars could be just part of the high angular-momentum tail of another Galactic component with a broader distribution of orbits, such as a prograde halo.

We would expect that, if they are part of an isotropic halo distribution, there would be the same number of stars with the same characteristics but on retrograde orbits. Figure 8 shows the action space for stars within the three databases with metallicities $-1.5 < [\mathrm{Fe/H}] < -1$ (top panels) and $[\mathrm{Fe/H}] < -1.5$ (bottom panels). A red continuous line at $L_z/J_{\mathrm{tot}} = 0$ separate stars on prograde (positive) and retrograde (negative) orbits. Shorter red dashed lines at $L_z/J_{\mathrm{tot}} = 0.8$ and -0.8 mark the most prograde (at the very end of which our thin-disc-like stars are located) and most retrograde extremes of the distributions. There is clearly an excess of stars on prograde orbits with respect to the retrograde counterpart. The *Gaia* RVS plot shows a striking lack of stars

compared with the other surveys, probably because the conservative selection cuts applied likely removed also bona fide metal-poor stars from our sample.

Recent simulations suggest that the galactic bar could induce the emergence of a stellar population on disc-like orbits initially belonging either to the halo (Dillamore et al. 2024) or to the inner galaxy (Yuan et al. 2023; Li et al. 2023). Our chemical analysis corroborates the fact that below [Fe/H] < −1 stars formed in a medium less chemically enriched than the bulk of the thick disc which could be the stellar halo. However, based on our results only, we cannot exclude the possibility of them being part of an ancient disc, formed before the majority of the thick disc.

The analysis performed by Zhang et al. (2023), fitting Gaussian mixture models to the 3D velocity space, revealed that below [Fe/H] < −1.6 there are no signs of a significant disc population (they limit it to <3% of their total distribution), which is in line with our findings. Like in this work (see the bottom plots of Fig. 8), they do find an asymmetry in rotational velocity at low metallicity (even for [Fe/H] < −2.0) with an excess of prograde stars, which they explained through the presence of a prograde halo component with a mean rotational velocity of ∼80 km s^{-1}. Further analyses with age distributions and/or more comprehensive chemical abundance measurements are required to clearly establish the precise metallicity at which the early Milky Way disc formed.

4. Conclusions and discussion

In this work, we have confirmed that the metallicity distribution of stars moving in thin-disc-like orbits, (i.e., with a high angular momentum, $L_z/J_{\rm tot} > 0.95$, moving very close to the plane, within $|Z_{\rm max}| < 750$ pc), shows a metal-poor tail that goes below the classical lower limit of [Fe/H] ∼ −0.7, and decreases at a constant rate in logarithmic scale down to [Fe/H] ∼ −1.5. Tentatively, we also found thin-disc-like stars at lower metallicities, down to [Fe/H] ∼ −2.5, although in much lower numbers.

Their orbital parameters show that they are confined to the plane, with the bulk of them having $|Z_{\rm max}| < 750$ pc (approximately twice the thin disc's scale height, e.g., Bland-Hawthorn & Gerhard 2016). This orbital distribution is observed independently on the metallicity range considered or their current location in the Galaxy. In particular, they are not restricted to the anticenter region where they were found for the first time by FA21, but cover the whole area surveyed by each database. However, we observed that the most metal-poor, those with [Fe/H] < −1.5, do not reach galactocentric radii larger than 10 kpc, suggesting that they do not belong to the outer disc. Dynamically selected thin-disc stars with −1 < [Fe/H] < −0.5 are comprised of both high- and low-α populations, but stars at lower metallicities are mostly high-α. The evaluation of the [Mg/Mn] vs. [Al/Fe] chemical space clearly shows that the chemically defined thin disc is initiated at metallicities between −1 < [Fe/H] < −0.7. Below [Fe/H] < −1, while the thin-disc-like stars show the chemical trends typical of an earlier chemical enrichment than the bulk of the thick disc.

Using *Gaia* and APOGEE data, Belokurov & Kravtsov (2022) found that MW stars formed in situ have a mean rotational velocity (and dispersion) variation with metallicity that could be explained by the formation of the disc from a kinematically hot spheroid of stars with a slightly net prograde rotation ($V_\phi = 50$ km s^{-1}), which spins up to the rotation of the current disc between −1.3 < [Fe/H] < −0.9. They interpret these findings as the transition from turbulent bursty star formation through gas accretion in cold narrow filaments to a more steady gas accretion phase through cooling gas from a hot halo that allows the formation of a coherent disc. They found that these in situ stars below [Fe/H] < −0.9 describe a broad velocity distribution that reaches velocities from −200 km s^{-1} to 300 km s^{-1}.

Following the Belokurov & Kravtsov (2022) scenario our metal-poor thin-disc-like stars could be the high angular-momentum tail of a thicker disc in formation. The fact that we see an increasing number of stars as a function of the metallicity moving in thin-disc-like orbits is coherent with the possibility of an incipient disc that gains angular momentum as the metallicity increases, because we would expect the number of high angular-momentum stars to also increase (Kordopatis et al. 2017). However, based on our results, such spin up might have started at lower metallicities, at least at [Fe/H] ∼ −1.5.

The evaluation of other chemical species would be helpful to verify whether they could belong to an accreted population. Recently, Mardini et al. (2022) pointed out the existence of metal-poor disc stars with metallicities lower than −0.8 dex down to −3.5 dex, that they called the Atari disc, for which they suggested an accreted origin. This stellar group was identified by selecting stars with similar characteristics as the "metal-weak" thick disc that had been previously detected (Norris et al. 1985; Ruchti et al. 2011; Kordopatis et al. 2013; Carollo et al. 2019). Although the Atari disc shares the same metallicity range with our metal-poor thin disc, there are significant differences between the two populations. The Atari disc mean rotational velocity is $\langle V_\phi \langle = 154$ km s^{-1}, which means that it rotates even slower than the thick disc, and, consequently, than our metal-poor thin disc. Atari stellar orbits are characterized by large eccentricities between $0.3 < ecc < 0.5$, typical of the halo and thick disc, contrary to our low eccentricity population, $ecc < 0.3$. It is true that these two populations were selected with different dynamical criteria, which explains why they do not show the same dynamical properties.

However, the analysis of the APOGEE chemical abundances has revealed that some of our selected stars may be indeed accreted. A further analysis will be the topic of future work. As mentioned in Sect. 3.2, chemical abundances derived with automatic pipelines that run on hundreds of thousands of stars have limitations. For this reason, a higher-resolution follow-up is planned to properly characterize these metal-poor thin-disc stars. For this sample (to come), reliable stellar ages will be also derived, as they are necessary to disentangle the origin of the Galactic disc populations.

Acknowledgements. The authors thank the anonymous referee for all the comments, which help to improve this work. They also acknoledge Patrick de Laverny for useful suggestions. EFA, GB and CG acknowledge support from the Agencia Estatal de Investigación del Ministerio de Ciencia e Innovación (AEI-MCINN) under grant "At the forefront of Galactic Archaeology: evolution of the luminous and dark matter components of the Milky Way and Local Group dwarf galaxies in the *Gaia* era" with reference PID2020-118778GB-I00/10.13039/501100011033. EFA also acknowledges support from the "María Zambrano" fellowship from the Universidad de La Laguna. GK, VH and IG gratefully acknowledge support from the french national research agency (ANR) funded project MWDisc (ANR-20-CE31-0004). AAA acknowledges support from the Herchel Smith Fellowship at the University of Cambridge and a Fitzwilliam College research fellowship supported by the Isaac Newton Trust. This research has been partially funded from a Spinoza award by NWO (SPI 78-411). This research was supported by the International Space Science Institute (ISSI) in Bern, through ISSI International Team project 540 (The Early Milky Way). This work has made use of data from the European Space Agency (ESA) mission *Gaia* (https://www.cosmos.esa.int/gaia), processed by the *Gaia* Data Processing and Analysis Consortium (DPAC, https://www.cosmos.esa.int/web/gaia/dpac/consortium). Funding for the DPAC has been provided by national institutions, in particular the institutions participating in the *Gaia* Multilateral Agreement. Funding for the Sloan Digital Sky

Survey IV has been provided by the Alfred P. Sloan Foundation, the US Department of Energy Office of Science, and the Participating Institutions. SDSS-IV acknowledges support and resources from the Center for High Performance Computing at the University of Utah. The SDSS website is www.sdss4.org. SDSS-IV is managed by the Astrophysical Research Consortium for the Participating Institutions of the SDSS Collaboration including the Brazilian Participation Group, the Carnegie Institution for Science, Carnegie Mellon University, Center for Astrophysics | Harvard & Smithsonian, the Chilean Participation Group, the French Participation Group, Instituto de Astrofísica de Canarias, The Johns Hopkins University, Kavli Institute for the Physics and Mathematics of the Universe (IPMU)/University of Tokyo, the Korean Participation Group, Lawrence Berkeley National Laboratory, Leibniz Institut für Astrophysik Potsdam (AIP), Max-Planck-Institut für Astronomie (MPIA Heidelberg), Max-Planck-Institut für Astrophysik (MPA Garching), Max-Planck-Institut für Extraterrestrische Physik (MPE), National Astronomical Observatories of China, New Mexico State University, New York University, University of Notre Dame, Observatário Nacional/MCTI, The Ohio State University, Pennsylvania State University, Shanghai Astronomical Observatory, United Kingdom Participation Group, Universidad Nacional Autónoma de México, University of Arizona, University of Colorado Boulder, University of Oxford, University of Portsmouth, University of Utah, University of Virginia, University of Washington, University of Wisconsin, Vanderbilt University, and Yale University. Collaboration Overview Affiliate Institutions Key People in SDSS Collaboration Council Committee on Inclusiveness Architects SDSS-IV Survey Science Teams and Working Groups Code of Conduct SDSS-IV Publication Policy How to Cite SDSS External Collaborator Policy For SDSS-IV Collaboration Members

References

Abadi, M. G., Navarro, J. F., Steinmetz, M., & Eke, V. R. 2003, ApJ, 591, 499
Abdurro'uf, Accetta, K., Aerts, C., et al. 2022, ApJS, 259, 35
Andrews, B. H., Weinberg, D. H., Schönrich, R., & Johnson, J. A. 2017, ApJ, 835, 224
Bailer-Jones, C. A. L., Rybizki, J., Fouesneau, M., Demleitner, M., & Andrae, R. 2021, AJ, 161, 147
Beers, T. C., Drilling, J. S., Rossi, S., et al. 2002, AJ, 124, 931
Belokurov, V., & Kravtsov, A. 2022, MNRAS, 514, 689
Bensby, T., Feltzing, S., & Lundström, I. 2003, A&A, 410, 527
Bensby, T., Feltzing, S., & Oey, M. S. 2014, A&A, 562, A71
Bird, J. C., Kazantzidis, S., Weinberg, D. H., et al. 2013, ApJ, 773, 43
Bland-Hawthorn, J., & Gerhard, O. 2016, ARA&A, 54, 529
Brook, C. B., Kawata, D., Gibson, B. K., & Freeman, K. C. 2004, ApJ, 612, 894
Buder, S., Sharma, S., Kos, J., et al. 2021, MNRAS, 506, 150
Carollo, D., Chiba, M., Ishigaki, M., et al. 2019, ApJ, 887, 22
Cordoni, G., Da Costa, G. S., Yong, D., et al. 2021, MNRAS, 503, 2539
Cropper, M., Katz, D., Sartoretti, P., et al. 2018, A&A, 616, A5
Das, P., Hawkins, K., & Jofré, P. 2020, MNRAS, 493, 5195
Dillamore, A. M., Belokurov, V., Kravtsov, A., & Font, A. S. 2024, MNRAS, 527, 7070
Di Matteo, P., Spite, M., Haywood, M., et al. 2020, A&A, 636, A115
Dovgal, A., Venn, K. A., Sestito, F., et al. 2024, MNRAS, 527, 7810
El-Badry, K., Bland-Hawthorn, J., Wetzel, A., et al. 2018, MNRAS, 480, 652
Fernández-Alvar, E., Carigi, L., Schuster, W. J., et al. 2018, ApJ, 852, 50
Fernández-Alvar, E., Kordopatis, G., Hill, V., et al. 2021, MNRAS, 508, 1509
Font, A. S., Navarro, J. F., Stadel, J., & Quinn, T. 2001, ApJ, 563, L1
Fuhrmann, K. 1998, A&A, 338, 161
Fuhrmann, K., Chini, R., Kaderhandt, L., & Chen, Z. 2017, MNRAS, 464, 2610
Gaia Collaboration (Prusti, T., et al.) 2016, A&A, 595, A1
Gaia Collaboration (Vallenari, A., et al.) 2023, A&A, 674, A1
Gilmore, G., & Reid, N. 1983, MNRAS, 202, 1025
Gilmore, G., Wyse, R. F. G., & Kuijken, K. 1989, ARA&A, 27, 555
GRAVITY Collaboration (Abuter, R., et al.) 2019, A&A, 625, L10
Hawkins, K., Jofré, P., Masseron, T., & Gilmore, G. 2015, MNRAS, 453, 758
Hayden, M. R., Holtzman, J. A., Bovy, J., et al. 2014, AJ, 147, 116
Hayden, M. R., Bovy, J., Holtzman, J. A., et al. 2015, ApJ, 808, 132
Horta, D., Schiavon, R. P., Mackereth, J. T., et al. 2021, MNRAS, 500, 1385
Hunt, E. L., & Reffert, S. 2023, A&A, 673, A114
Imig, J., Price, C., Holtzman, J. A., et al. 2023, ApJ, 954, 124
Jones, B. J. T., & Wyse, R. F. G. 1983, A&A, 120, 165
Jönsson, H., Holtzman, J. A., Allende Prieto, C., et al. 2020, AJ, 160, 120
Jurić, M., Ivezić, Ž., Brooks, A., et al. 2008, ApJ, 673, 864
Katz, D., Soubiran, C., Cayrel, R., et al. 2011, A&A, 525, A90
Kordopatis, G., Recio-Blanco, A., de Laverny, P., et al. 2011a, A&A, 535, A106
Kordopatis, G., Recio-Blanco, A., de Laverny, P., et al. 2011b, A&A, 535, A107
Kordopatis, G., Gilmore, G., Wyse, R. F. G., et al. 2013, MNRAS, 436, 3231
Kordopatis, G., Wyse, R. F. G., Gilmore, G., et al. 2015, A&A, 582, A122
Kordopatis, G., Wyse, R. F. G., Chiappini, C., et al. 2017, MNRAS, 467, 469
Kordopatis, G., Recio-Blanco, A., Schultheis, M., & Hill, V. 2020, A&A, 643, A69
Kordopatis, G., Schultheis, M., McMillan, P. J., et al. 2023, A&A, 669, A104
Li, C., Yuan, Z., Monari, G., et al. 2023, A&A, submitted [arXiv:2311.15270]
Lindegren, L., Bastian, U., Biermann, M., et al. 2021, A&A, 649, A4
Mardini, M. K., Frebel, A., Chiti, A., et al. 2022, ApJ, 936, 78
Martin, N. F., Starkenburg, E., Yuan, Z., et al. 2023, A&A, submitted [arXiv:2308.01344]
Matsuno, T., Starkenburg, E., Balbinot, E., & Helmi, A. 2022, arXiv e-prints [arXiv:2212.11639]
McMillan, P. J. 2017, MNRAS, 465, 76
Mikolaitis, Š., Hill, V., Recio-Blanco, A., et al. 2014, A&A, 572, A33
Norris, J., Bessell, M. S., & Pickles, A. J. 1985, ApJS, 58, 463
Prantzos, N., Abia, C., Chen, T., et al. 2023, MNRAS, 523, 2126
Queiroz, A. B. A., Anders, F., Chiappini, C., et al. 2020, A&A, 638, A76
Quinn, P. J., Hernquist, L., & Fullagar, D. P. 1993, ApJ, 403, 74
Recio-Blanco, A., de Laverny, P., Kordopatis, G., et al. 2014, A&A, 567, A5
Recio-Blanco, A., de Laverny, P., Palicio, P. A., et al. 2023, A&A, 674, A29
Reddy, B. E., Tomkin, J., Lambert, D. L., & Allende Prieto, C. 2003, MNRAS, 340, 304
Ruchti, G. R., Fulbright, J. P., Wyse, R. F. G., et al. 2011, ApJ, 737, 9
Santistevan, I. B., Wetzel, A., Sanderson, R. E., et al. 2021, MNRAS, 505, 921
Sestito, F., Longeard, N., Martin, N. F., et al. 2019, MNRAS, 484, 2166
Sestito, F., Martin, N. F., Starkenburg, E., et al. 2020, MNRAS, 497, L7
Sestito, F., Buck, T., Starkenburg, E., et al. 2021, MNRAS, 500, 3750
Starkenburg, E., Martin, N., Youakim, K., et al. 2017, MNRAS, 471, 2587
Tolstoy, E., Hill, V., & Tosi, M. 2009, ARA&A, 47, 371
Venn, K. A., Kielty, C. L., Sestito, F., et al. 2020, MNRAS, 492, 3241
Vieira, K., Korchagin, V., Carraro, G., & Lutsenko, A. 2023, Galaxies, 11, 77
Villalobos, Á., & Helmi, A. 2008, MNRAS, 391, 1806
Yuan, Z., Li, C., Martin, N. F., et al. 2023, A&A, submitted [arXiv:2311.08464]
Zhang, H., Ardern-Arentsen, A., & Belokurov, V. 2023, MNRAS, submitted [arXiv:2311.09294]

Appendix A: Flags quality selection on *Gaia* RVS.

Table A.1. Flags and stellar parameters of the stars selected in our *Gaia* RVS sample.

flag_vbroadT	0,1
flag_vbroadG	0,1
flag_vbroadM	0,1
flag_vradT	0,1
flag_vradG	0,1
flag_vradM	0,1
flag_fluxnoise	0,1, and 2 where [Fe/H][8]< -2
flag_extrapol	0,1
flag_negflux	0
flag_nanflux	0
flag_emission	0
flag_nullfluxer	0
flag_KM	0
spectraltype_esphs	all except type O, B and A
$T_{\rm eff}$ (K)	[4250, 6000]
$\log g$ (dex)	[0, 4.75]

[8] Uncalibrated *Gaia* RVS [M/H]

Appendix B: *Gaia* RVS [Fe/H] comparison with APOGEE and GALAH [Fe/H].

Figure B.1 shows the metallicity comparison of calibrated *Gaia* RVS DR3 measurements with respect to the GALAH DR3 and APOGEE DR17 determinations, color coded with the [α/Fe] ratios measured in *Gaia* RVS. We see that there is a dependence of the [Fe/H] deviations with the [α/Fe]: stars with very large [Fe/H] discrepancies correspond to objects with high [α/Fe]. After an inspection of the flags provided by the *Gaia* Collaboration in Recio-Blanco et al. (2023), we realized that the comparison of *Gaia* RVS [Fe/H] with APOGEE and GALAH are much improved by selecting stars with *flags_gspspec* chain character number 7 (hereafter *fluxnoise_flag*) < 2. The reason why this flag helps to improve the comparison with GALAH and APOGEE estimates is because it warns us of the flux noise-induced uncertainties (Recio-Blanco et al. 2023). When it is equal to 2, the uncertainties in [Fe/H] are estimated to be $0.25 < \sigma$[Fe/H] ≤ 0.5, being lower than 0.25 for stars flagged below < 2.

In the case of stars with uncalibrated *Gaia* RVS [Fe/H] < -2, we see that overall, after calibration, they are in fairly good agreement with the GALAH and APOGEE measurements, even those with *fluxnoise_flag* = 2. There is, however, a negative offset in *Gaia* RVS [Fe/H] respect to the other surveys. In particular in GALAH, the comparison in this metallicity range shows a relatively large standard deviation. Still, because stars below [Fe/H] < -2 are scarce and that even with the negative offset and standard deviation, they will remain with a metallicity below the thin-disc metal-poor limit we are evaluating, [Fe/H] < -0.55, we decided to keep them all. The big circles in Figure B.1 show the [Fe/H] comparison of stars after applying the final selection of flags and the mean differences in [Fe/H] and standard deviations at several metallicity ranges are collected in Table B.1.

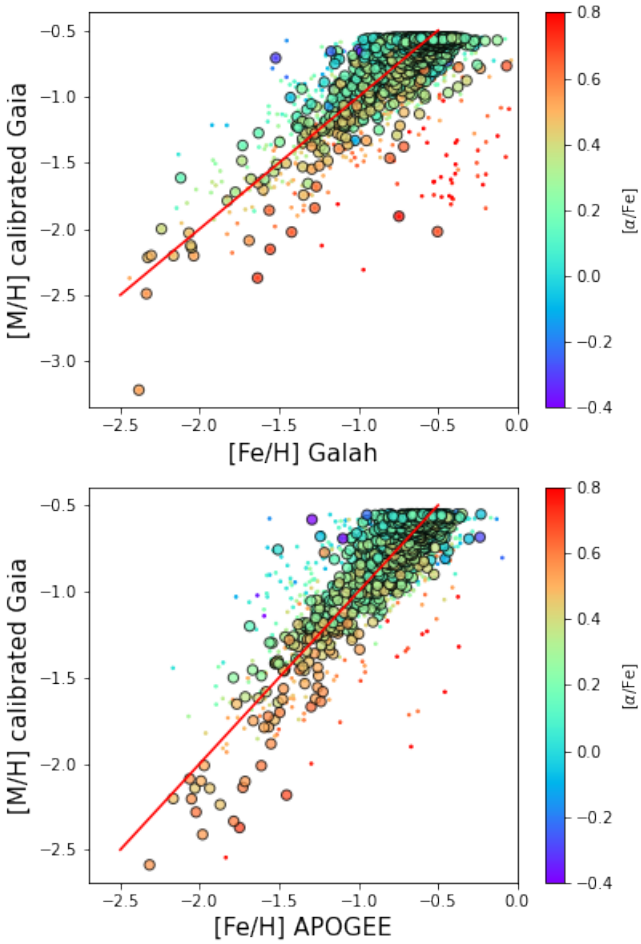

Fig. B.1. Calibrated *Gaia* DR3 RVS [Fe/H] as a function of [Fe/H] estimates from GALAH DR3 (top panel) and APOGEE DR17 (bottom panel) of stars with [Fe/H] < -0.5 that pass the quality selection criteria. Small and big circles show stars before and after removing stars with *Gaia* DR3 RVS [Fe/H] > -2 and the *fluxnoise_flag* = 2, respectively. The color code indicates the [α/Fe] *Gaia* RVS DR3 measurements between for each star.

Table B.1. Mean and standard deviations of the [Fe/H] differences between the measurements provided by *Gaia* RVS and those by GALAH or APOGEE, after applying all the quality cuts.

Calibrated *Gaia* RVS [Fe/H]	$< \Delta_{\rm GALAH} > \pm\sigma$	$< \Delta_{\rm APOGEE} > \pm\sigma$
(-3,-2)	-0.40 ± 0.63	-0.30 ± 0.20
(-2,-1.5)	-0.18 ± 0.33	-0.15 ± 0.18
(-1.5,-1)	-0.07 ± 0.20	-0.01 ± 0.13
(-1.5,-0.55)	-0.02 ± 0.13	0.01 ± 0.11